High-pressure phases of boron pnictides BX (X = As, Sb, Bi) with quartz topology from first principles

Vladimir Solozhenko, Samir Matar

High-pressure phases of boron pnictides BX (X = As, Sb, Bi) with quartz topology from first principles

Vladimir L. Solozhenko * https://orcid.org/0000-0002-0881-9761

LSPM–CNRS, Université Sorbonne Paris Nord, 93430 Villetaneuse, France

Samir F. Matar https://orcid.org/0000-0001-5419-358X

Lebanese German University (LGU), Sahel Alma, Jounieh, Lebanon

Abstract

The superdense hexagonal boron pnictides BX (X = As, Sb, Bi), whose structures are formed by distorted tetrahedra and characterized by a quartz-derived (**qtz**) topology, have been predicted from first principles as potential high-pressure phases. From full geometry structure relaxation and ground state energy calculations based on quantum density functional theory (DFT), **qtz** BX were found to be mechanically (elastic constants) and dynamically (phonons) stable. From the energy-volume equations of state, at experimentally accessible pressures **qtz** boron pnictides were found to be more energetically favorable than corresponding cubic zinc-blende phases with diamond-like (**dia**) topology. According to the electronic band structures, the zinc-blende BX have larger band gaps than the **qtz** phases, which can be attributed to the higher covalence of the latter. A metallic behavior is only observed for **qtz** BBi, which is related to the dynamic instability as it follows from the phonon band structure.

Keywords: boron pnictides; high pressure; topology; DFT; equation of state; elastic constants; phonons

* Corresponding author (vladimir.solozhenko@univ-paris13.fr)

1. Introduction

III-V compound semiconductors provide the material basis for a number of well-established technologies and new classes of advanced high-temperature, high-power and high-frequency electronic/optoelectronic devices such as high-electron-mobility heterostructures, light-emitting diodes, diode lasers, electro-optic modulators, photodetectors, frequency-mixing modules, etc. [1].

Among the A^{III}-B^{V} semiconductors, boron monopnictides are interesting because of their unique behavior due to the small size of the boron atom and the absence of p-electrons. The most studied compounds in this group are boron nitride (BN) and boron phosphide (BP). Boron arsenide (BAs) is much less studied experimentally (see recent review [2] and references therein), while BSb and BBi have not yet been synthesized, and have been studied only by theoretical methods [3-7].

Theoretical studies of BAs at high pressure have so far been mainly limited to the consideration of the phase with rocksalt structure [5,7-14]. Wentzcovitch *et al*. [8] have studied the relative stability of different BAs phases using the total-energy pseudopotential technique and reported structural transition from fourfold coordinated zinc-blende (*zb*) phase to sixfold coordinated rocksalt (*rs*) phase at 110 GPa. According to other works [9-14], the transition pressure varies from 93 GPa [13] to 134 GPa [9]. However, this transition has never been observed experimentally; on the contrary, it was found that BAs undergoes a collapse from the zinc-blende phase to an amorphous state at pressures above 125 GPa [15]. As for the hypothetical high-pressure phases with β-Sn and CsCl structure, they were found to be less energetically favorable than the rocksalt phase of BAs [8].

Phase diagrams of the B-Sb [16] and B-Bi [17] systems at ambient pressure have a similar topology, characterized by the absence of binary compounds and the presence of noninvariant reactions of decomposition of the liquid phase into β-rhombohedral boron and a vapor phase. Therefore, zinc-blende BSb and BBi, which have been claimed to be the ground-state phases [3-7], are hypothetical. The same is true for their high-pressure transitions to corresponding rocksalt phases.

The structures of the currently known zinc-blende boron pnictides (BN, BP and BAs), have **dia** topology (as cubic diamond) [18], which is characterized by the spatial arrangement of BN_4, BP_4 or BAs_4 perfect (angle ∠109.47°) sp^3-like corner-sharing tetrahedra in three-dimensional 3D nets (cf. Fig. 1a). Recently, we discovered a significant structural densification of zinc-blende BN and BP by adopting a quartz-derived structure (**qtz** topology) characterized by distorted corner-sharing BN_4 and BP_4 tetrahedra [19,20].

In this context, the present work extends our investigation to boron pnictides with heavier elements (As, Sb, and Bi). As in previous works [19,20], the studies are based on quantum mechanics calculations of the ground-state energy structures and derived properties in the framework of the density functional theory (DFT) [21,22]. It is shown that BX phases (X = As, Sb, Bi) with **qtz** topology are cohesive and stable both mechanically (elastic constants and their combinations) and dynamically (phonon band structures). It should be noted, however, that there is a small dynamical instability of **qtz** BX in the case of the heaviest pnictogen, bismuth. The respective equations of

state (EOS) have been determined for all phases, and the transition pressures from *zb*-BX to the corresponding high-pressure **qtz** structures have been estimated. The electronic band structures show a reduction of the band gaps in the proposed **qtz** phases compared to *zb*-BX, with metallization observed in the case of **qtz** BBi. Finally, the thermodynamic properties (heat capacity and entropy) of the new phases have been calculated and compared with the available experimental data.

2. Computational methodology

The identification of the ground state structures corresponding to the energy minima and the prediction of their mechanical and dynamical properties were carried out by DFT-based calculations using the Vienna Ab initio Simulation Package (VASP) code [23,24] and the projector augmented wave (PAW) method [24,25] for the atomic potentials. DFT exchange correlation (XC) effects were taken into account using the generalized gradient functional approximation (GGA) [26]. Preliminary calculations with the original DFT-XC local density approximation (LDA) [27] resulted in underestimated lattice constants of *zb*-BX at ambient pressure and were subsequently abandoned. The atoms were relaxed to the ground state structures using the conjugate gradient algorithm according to Press *et al*. [28]. The Blöchl tetrahedron method [29] with corrections according to the Methfessel and Paxton scheme [30] was used for geometry optimization and energy calculations, respectively. Brillouin-zone integrals were approximated by a special **k**-point sampling according to Monkhorst and Pack [31]. Structural parameters were optimized until atomic forces were below 0.02 eV/Å and all stress components were < 0.003 eV/Å^3. The calculations were converged at an energy cutoff of 400 eV for the plane-wave basis set in terms of the **k**-point integration in the reciprocal space from $k_x(6)\times k_y(6)\times k_z(6)$ up to $k_x(12)\times k_y(12)\times k_z(12)$ for *zb*-BX and $k_x(6)\times k_y(6)\times k_z(4)$ up to $k_x(12)\times k_y(12)\times k_z(8)$ for **qtz** BX to obtain a final convergence and relaxation to zero strains. In the post-processing of the ground state electronic structures, the charge density projections were operated on the lattice sites.

The mechanical stability was evaluated from the elastic constants calculations. The analysis of the elastic tensors was carried out using the ELATE software [32], which provides the bulk (B), shear (G) and Young's (E) moduli along different averaging methods; the Voigt approach [33] was chosen here. Vickers hardness (H_V) from elastic properties was evaluated using the empirical Mazhnik-Oganov [34] and Chen-Niu [35] models. The hardness was also estimated using the thermodynamic model, which is based on thermodynamic properties and crystal structure [36], and the Lyakhov-Oganov approach [37], which considers the topology of the crystal structure, the strength of covalent bonds, the degree of ionicity and directionality. The fracture toughness (K_{Ic}) was evaluated within the Mazhnik-Oganov model [34].

The dynamic stabilities of the considered boron pnictides were confirmed by the positive values of phonon frequencies. The corresponding phonon band structures were obtained according to Togo and Tanaka [38]. Thermodynamic properties (heat capacity at constant volume C_V and entropy S)

were calculated from the phonon frequencies using the statistical thermodynamics on a high precision sampling mesh in the Brillouin zone [39].

The electronic band structures were obtained using the all-electron DFT-based ASW method [40] and the GGA XC functional [26]. The VESTA (Visualization for Electronic and STructural Analysis) software [41] was used to visualize the crystal structures and charge densities.

3. Results and Discussion

3.1 Crystal chemistry

The preliminary computations consisted of calculating the structures of *zb*-BX to reproduce the experimental [42] and theoretical [43] findings. Table 1 shows the calculated and available experimental lattice constants *a* of *zb*-BAs which are in good agreement. The zinc-blende structure is shown in Fig. 1 in a ball-and-stick and tetrahedral representations. The latter shows that the tetrahedra are regular as in diamond, presenting the sp^3-like $\angle 109.47°$ angle as mentioned above, with only B–As bonds. The observation is relevant in that the **qtz** topology is characterized by distorted tetrahedra.

Recently we reported a novel **qtz** C_6 belonging to space group $P6_522$ (No. 179) with a single 6-fold Wyckoff position [44]. To consider binary compounds, it was necessary to change the space group to $P6_222$ (No. 180), with a splitting into two 3-fold Wyckoff positions. The results of the unconstrained geometry optimizations are shown in Table 1. A comparison of *zb*-BX (X = As, Sb, Bi) shows a systematic decrease in volume as per formula unit (FU), which suggests densification. However, the shortest interatomic distance is systematically larger in **qtz** BX than in *zb*-BX, accompanied by the presence of distorted tetrahedra with angles smaller and larger than the ideal angle of 109.47°. The total energy per FU is lower (higher in absolute value) in **qtz** BX than in *zb*-BX. This observation is expected from the fact that *zb*-BX phases are the ground state structures with $\Delta E/F$, largest for X = As versus X = Bi. These results, which show denser **qtz** BX phases with smaller volumes and higher energies than those for *zb*-BX, suggest that **qtz** BX are potential high-pressure phases, as will be shown below.

In terms of chemical behavior, with the χ symbol denoting Pauling electronegativity, $\chi B = 2.04$ on the one hand, and $\chi As = 2.19$, $\chi Sb = 2.05$, and $\chi Bi = 2.02$ on the other. Based on $\Delta\chi$, BAs can be considered ionocovalent with $\Delta\chi(BAs) = 0.15$, while the other two boron pnictides characterized by $\Delta\chi(BSb) = 0.01$ and $\Delta\chi(BBi) = 0.02$ should be considered covalent.

3.2 Mechanical properties

The mechanical behavior of boron pnictides has been analyzed by calculating the elastic properties by performing finite distortions of the lattice. The calculated sets of elastic constants C_{ij} (i and j correspond to directions) for zinc-blende and **qtz** phases are given in Table 2. All C_{ij} values are

positive, indicating mechanically stable phases. **qtz** pnictides have systematically larger C_{11}, C_{33} and C_{66} values than corresponding zinc-blende polymorphs due to the smaller volumes per formula unit. Along the BAs - BSb - BBi series, there is a tendency for the C_{ij} values of zinc-blende and **qtz** phases to decrease due to the increase in atomic radii: r(As) = 1.2 Å, r(Sb) = 1.4 Å, r(Bi) = 1.5 Å, and consequently to increase in cell volume and compressibility.

The bulk (B_V), shear (G_V) and Young's (E_V) moduli were then obtained by Voigt averaging [33] the elastic constants using ELATE software [32]. The last three columns of Table 2 show the elastic moduli with values that follow the trends observed for C_{ij}.

It should be noted that the bulk modulus of *zb*-BAs calculated from the elastic constants (134 GPa) is ~10% smaller than the experimental values obtained by synchrotron X-ray diffraction study (148(6) GPa [15]) and picosecond interferometry (148(9) GPa [45]). On the other hand, the B_0 value of 146 GPa calculated in the framework of the thermodynamic model [36] is in perfect agreement with the experimental data. For this reason, the bulk modulus values obtained using the thermodynamic model (see Table 3) should be preferred also for all other pnictides.

The Vickers hardness (H_V) values of all considered boron pnictides, calculated using four contemporary models [34-37], are summarized in Table 3. For *zb*-BAs, all models except the empirical Chen-Niu model give hardness values that are in good agreement with the experimental value of 22(3) GPa [46]. For BSb and BBi, there is a significant divergence of H_V values calculated by different models (see Table 3), and the nature of these divergences indicates that in this case all models except the thermodynamic one [36] can be considered unreliable. Previously, we observed a similar situation for the superhard phases of the B-C-N system [47]. Based on the hardness values calculated using the thermodynamic model, we can conclude that in the BAs - BSb - BBi series, the Vickers hardness decreases from 24 to 15 GPa, with practically no differences observed between zinc-blende and **qtz** polymorphs. In any case, all considered boron pnictides are hard phases with Vickers hardness exceeding that of cemented tungsten carbide, the conventional hard material.

The fracture toughness of *zb*-BAs evaluated within the Mazhnik-Oganov model [34], K_{Ic} = 1.4 MPa·m^{½}, agrees well with the experimental value of 1.2 MPa·m^{½} [46], indicating that cubic boron arsenide (as well as **qtz** polymorph) is more brittle than cubic BN (2.8 MPa·m^{½} [48]) and cubic BP (1.8 MPa·m^{½} [49]). Hypothetical boron antimonide and boron bismuthate (both zinc-blende and **qtz** polymorphs) were found to be even more brittle (see Table 3).

3.3 Equations of state and possible high-pressure phase transitions

When considering different structures of crystalline solids, comparative energy trends can be determined from their equations of state (EOS). This was done based on a series of calculations of total energy as a function of volume for the zinc-blende and **qtz** BX phases. The resulting E(V) curves, shown in Fig. 2, were fitted to the third-order Birch equations of state [50]:

$$E(V) = E_0(V_0) + (9/8)\cdot V_0 B_0[([(V_0)/V])^{2/3} - 1]^2 + (9/16)\cdot B_0(B_0' - 4)V_0[([(V_0)/V])^{2/3} - 1]^3,$$

where E_0, V_0, B_0 and B_0' are the equilibrium energy, volume, bulk modulus and its first pressure derivative, respectively. The calculated values for the static properties, and the transition pressures and reduced volumes are summarized in Table 4.

In the case of boron arsenide (Fig. 2a), the intersection of $E(V)$ curves of zinc-blende and **qtz** phases is observed at V/FU = 19.0 Å, which for *zb*-BAs is equivalent to a reduced volume of 0.697. The corresponding pressure can be calculated from the Murnaghan equation [51]

$$p = B_0/B_0' [(V_0)/V])^{B_0'} - 1]$$

using the experimental values of B_0, B_0' and V_0 (Table 4), and is equal to 117 GPa. Thus, it can be assumed that the pressure-induced phase transition from *zb*-BAs to **qtz** BAs can occur at pressures not lower than 117 GPa, which is consistent with the experimental data on the absence of room-temperature phase transitions of *zb*-BAs up to 125 GPa [15].

For two other boron pnictides, the intersections of the $E(V)$ curves of *zb*-BX and **qtz** BX are observed at $V/V_0 = 0.724$ for *zb*-BSb (Fig. 2b) and $V/V_0 = 0.763$ for *zb*-BBi (Fig. 2c). The corresponding pressures, 71 GPa and 51 GPa, were estimated using the most reliable B_0 values calculated in framework of the thermodynamic model (Table 4), while B_0' values were fixed at 4.

Thus, with increasing pnictogen atomic number, a drastic decrease in the *zb*-to-**qtz** transition pressure is observed from 144 GPa for BP [20] down to 51 GPa for BBi.

3.4 Dynamic and thermodynamic properties from the phonons

To verify the dynamical stability of the predicted phases, their phonon properties were studied. The phonon band structures (red lines) obtained according to the protocol presented in section 2 are shown in Fig. 3. The horizontal direction corresponds to the main directions of the hexagonal Brillouin zone, while the vertical direction shows the frequencies ω, given in terahertz (THz). The absence of negative frequencies indicates dynamically stable phases. The band structure includes 3N bands with 3N-3 optical modes found at higher energies than three acoustic modes starting from zero energy (ω = 0) at the Γ point, the center of the Brillouin zone, up to a few terahertz. They correspond to the lattice rigid translation modes of the crystal (two transverse and one longitudinal). Five panels in Fig. 3(a-e) show all positive frequency values, while for **qtz** BBi (Fig. 3f) negative phonon curves are observed along most of the Brillouin zone directions. *zb*-BBi, however, shows no such negative phonons. This indicates an instability of the longitudinal acoustic mode in **qtz** BBi which may result from drastic changes in the electronic structure as described below.

The thermodynamic properties of the boron pnictides were calculated from the phonon frequencies using the statistical thermodynamic approach [39] on a high-precision sampling mesh in the Brillouin zone. The temperature dependencies of heat capacity at constant volume (C_v) and entropy

(S) of zinc-blende and **qtz** BAs are shown in Fig. 4a in comparison with experimental C_p data for *zb*-BAs [2,52]. The observed excellent agreement between the calculated and experimental data indicates the validity of the method used to estimate the thermodynamic properties for the case of boron pnictides. For all three compounds, the heat capacity and entropy of **qtz** BX phases are slightly higher than those of *zb*-BX (Fig. 4), which is expected for structures containing distorted corner-sharing tetrahedra compared to the ideal zinc-blende structure.

3.5 Electronic band structures

Using the crystal parameters in Table 1, the electronic band structures were calculated using the all-electrons DFT-based augmented spherical method (ASW) [40]. The results are shown in Fig. 5. The bands (blue lines) develop along the main directions of the respective Brillouin zones, i.e. cubic for *zb*-BX and hexagonal for **qtz** BX. In all panels, except for Fig. 5f corresponding to **qtz** BBi, the zero energy along the vertical axis is considered with respect to E_V, at the top of the filled valence band (VB), separated from the empty conduction band (CB) by a small band gap. For all three boron pnictides, the zinc-blende phases have larger band gaps compared to the **qtz** phases. The smaller magnitudes for the latter result from the smaller volumes per formula unit, leading to an increased covalence. Within the same structure, going from BAs to BSb and then to BBi, the covalent character of the phase increases, as shown above with the Pauling electronegativity values χ and their differences $\Delta\chi$ for the considered boron pnictides. As a result, the energy gap within the zinc-blende BX series decreases. The same is observed for high-pressure **qtz** BX, but the pressure has already reduced the band gap of all these phases, and finally there is a total closing of the band gap in **qtz** BBi, which behaves as a metal with the energy reference at the Fermi level E_F. The transition from semiconducting *zb*-BBi to metallic **qtz** BBi can be proposed to explain the dynamic instability observed from the phonons

4. Conclusions

Based on crystal chemistry and density functional theory calculations, superdense hexagonal ($P6_422$) boron pnictides BX (X = As, Sb, Bi) with quartz-derived topology were predicted as possible high-pressure phases. The new hexagonal **qtz** BX phases were found to be cohesive, with higher energies than the cubic zinc-blende (F-43m) polymorphs, but they tend to predominate at low volumes (high pressures). The transition pressures calculated from the corresponding energy-volume E(V) equations of state are 117 GPa (BAs), 71 GPa (BSb), and 51 GPa (BBi). In addition to mechanical stability from elastic constants, the **qtz** BX phases are also dynamically stable as indicated by the phonon band structures. The heat capacities of the **qtz** phases calculated from the phonon frequencies were found to be slightly higher than those of the corresponding zinc-blende phases which is quite expected for structures containing distorted corner-sharing tetrahedra. From the analysis of the electronic band structures, it was found that all zinc-blende boron pnictides have

larger band gaps than the corresponding **qtz** phases, which can be attributed to an increased covalence due to the higher density of the latter. A special feature observed for metallic **qtz** BBi is related to the dynamic instability observed from the phonon band structure.

References

1. Vurgaftman, I.; Meyer, J.R.; Ram-Mohan, L.R. Band parameters for III–V compound semiconductors and their alloys. *Appl. Phys. Rev*. **2001**, *89*, 5815-5875.
2. Kang, J.S.; Li, M.; Wu, H.; Nguyen, H.; Hua, Y. Basic physical properties of cubic boron arsenide. *Appl. Phys. Lett.* **2019**, *115*, 122103.
3. Ferhat, M.; Bouhafs, B.; Zaoui, A.; Aourag, H. First-principles study of structural and electronic properties of BSb. *J. Phys.: Condens. Matter* **1998**, *10*, 7995.
4. Zaoui, A.; Ferhat, M. High-pressure structural phase transition of BSb. *Phys. Stat. Sol. (b)* **2001**, *225*, 15-19.
5. Ustundag, M.; Aslan, M.; Yalcin, B.G. The first-principles study on physical properties and phase stability of Boron-V (BN, BP, BAs, BSb and BBi) compounds. *Comput. Mater. Sci*. **2014**, *81*,
6. Bioud, N.; Sun, X.-W.; Daoud, S.; Song, T.; Zi-Jiang Liu, Z.-J. Structural stability and thermodynamic properties of BSb under high pressure and temperature. *Mater. Res. Express* **2018**, *5*, 085904.
7. Mujica, A.; Rubio, A.; Munoz, A.; Needs, R.J. High-pressure phases of group-IV, III–V, and II–VI compounds. *Rev. Mod. Phys.* **2003***, 75*, 863-912.
8. Wentzcovitch, R.M.; Cohen, M.L.; Lam, P.K. Theoretical study of BN, BP, and BAs at high pressures. *Phys. Rev. B* **1987**, *36*, 6058-6068.
9. Cui, S.; Feng, W.; Hua, H.; Feng, Z.; Wang, Y. First-principles study of zinc-blende to rocksalt phase transition in BP and BAs. *Comput. Mater. Sci.* **2009**, *44*, 1386–1389
10. Lu, B.; Linghu, R.-F.; Yi, Y.; Yang, X.-D. Characterisation of the high-pressure structural transition and elastic properties in boron arsenic. *Chin. Phys. B* **2010**, *19*, 076201.
11. Varshney, D.; Joshi, G.; Varshney, M.; Shriya, S. Pressure induced mechanical properties of boron based pnictides. *Solid State Sci.* **2010**, *12*, 864-872.
12. Talati, M.; Jha; P.K. Structural phase transition in boron compounds at high pressure. *Int. J. Mod. Phys. B* **2010**, *24*, 1235-1244.
13. Sarwan, M.; Bhardwaj, P.; Singh, S. Zinc-blende to rock-salt structural phase transition of BP and BAs under high pressure. *Chem. Phys.* **2013**, *426*, 1-8.
14. Daoud, S.; Bioud, N.; Bouarissa, N. Structural phase transition, elastic and thermal properties of boron arsenide: Pressure-induced effects. *Mater. Sci. Semicond. Process.* **2015**, *31*, 124-130.

15. Greene, R.G.; Luo, H.; Ruoff, A.L.; Trail, S.S.; DiSalvo F.J. Pressure induced metastable amorphization of BAs: Evidence for a kinetically frustrated phase transformation. *Phys. Rev. Lett.* **1994**, *73*, 2476-2479.

16. Okamoto, H. BSb (BoronAntimony). *J. Phase Equil.* **1991**, *125*, 391-393.

17. Okamoto, H. B-Bi (Boron-Bismuth). *J. Phase Equil.* **1991**, *125*, 391.

18. Alexandrov, E.V.; Blatov, V.A.; Kochetkov, A.V.; Proserpio, D.M. Underlying nets in three-periodic coordination polymers: topology, taxonomy and prediction from a computer-aided analysis of the Cambridge Structural Database. *CrystEngComm* **2011**, *13*, 3947-3958.

19. Matar, S.F.; Solozhenko, V.L. Ultrahigh-density superhard hexagonal BN and SiC with quartz topology from crystal chemistry and first principles. *Crystals* **2023**, *13*, 1498.

20. Solozhenko, V.L.; Matar, S.F. Superdense hexagonal BP and AlP with quartz topology: Crystal chemistry and DFT study. *Crystals* **2023**, *13*, 1622.

21. Hohenberg, P.; Kohn, W. Inhomogeneous electron gas. *Phys. Rev. B* **1964**, *136*, 864-871.

22. Kohn, W.; Sham, L.J. Self-consistent equations including exchange and correlation effects. *Phys. Rev. A* **1965**, *140*, 1133-1138.

23. Kresse, G.; Furthmüller, J. Efficient iterative schemes for ab initio total-energy calculations using a plane-wave basis set. *Phys. Rev. B* **1996**, *54*, 11169.

24. Kresse, G.; Joubert, J. From ultrasoft pseudopotentials to the projector augmented wave. *Phys. Rev. B* **1999**, *59*, 1758-1775.

25. Blöchl, P.E. Projector augmented wave method. *Phys. Rev. B* **1994**, *50*, 17953-17979.

26. Perdew, J.; Burke, K.; Ernzerhof, M. The Generalized Gradient Approximation made simple. *Phys. Rev. Lett.* **1996**, *77*, 3865-3868.

27. Ceperley, D.M.; Alder, B.J. Ground state of the electron gas by a stochastic method. *Phys. Rev. Lett.* **1980**, *45*, 566-569.

28. Press, W.H.; Flannery, B.P.; Teukolsky, S.A.; Vetterling, W.T. Numerical Recipes, 2nd ed.; Cambridge University Press: New York, USA, 1986.

29. Blöchl, P.; Jepsen, O.; Anderson, O. Improved tetrahedron method for Brillouin-zone integrations. *Phys. Rev. B* **1994**, *49*, 16223-16233.

30. Methfessel, M.; Paxton, A.T. High-precision sampling for Brillouin-zone integration in metals. *Phys. Rev. B* **1989**, *40*, 3616–3621.

31. Monkhorst, H.J.; Pack, J.D. Special k-points for Brillouin Zone integration. *Phys. Rev. B* **1976**, *13*, 5188-5192.

32. Gaillac, R.; Pullumbi, P.; Coudert, F.X. ELATE: an open-source online application for analysis and visualization of elastic tensors. *J. Phys.: Condens. Matter* **2016**, *28*, 275201.

33. Voigt, W. Über die Beziehung zwischen den beiden Elasticitätsconstanten isotroper Körper. *Annal. Phys.* **1889**, *274*, 573-587.

34. Mazhnik, E.; Oganov, A.R. A model of hardness and fracture toughness of solids. *J. Appl. Phys.* **2019**, *126*, 125109.

35. Chen, X.Q.; Niu, H.; Li, D.; Li, Y. Modeling hardness of polycrystalline materials and bulk metallic glasses. *Intermetallics* **2011**, *19*, 1275-1281.

36. Mukhanov, V.A.; Kurakevych, O.O.; Solozhenko, V.L. The interrelation between hardness and compressibility of substances and their structure and thermodynamic properties. *J. Superhard Mater.* **2008**, *30*, 368-378.

37. Lyakhov, A.O.; Oganov, A.R. Evolutionary search for superhard materials: Methodology and applications to forms of carbon and TiO_2. *Phys. Rev. B* **2011**, *84*, 092103.

38. Togo, A.; Tanaka, I. First principles phonon calculations in materials science, *Scr. Mater.* **2015**, *108*, 1-5.

39. Dove, M.T. Introduction to lattice dynamics. Cambridge University Press: New York, USA, 1993.

40. Eyert, V. Basic notions and applications of the augmented spherical wave method. *Int. J. Quantum Chem.* **2000**, *77*, 1007-1031.

41. Momma, K.; Izumi, F. VESTA3 for three-dimensional visualization of crystal, volumetric and morphology data. *J. Appl. Crystallogr.* **2011**, *44*, 1272-1276.

42. Eliseev, A.A.; Babitsyuna, A.A.; Medvedeva, Z.S. X-ray investigation of the arsenic-boron system. *Russ. J. Inorg. Chem.* **1964**, *9*, 633-636.

43. Schowalter, M.; Rosenauer, A.; Volz, K. Parameters for temperature dependence of mean-square displacements for B-, Bi- and Tl-containing binary III-V compounds. *Acta Crystallogr. A* **2012**, *68*, 319-323.

44. Matar, S.F.; Solozhenko, V.L. First principles search for novel ultrahard high-density carbon allotropes: hexagonal C_6, C_9 and C_{12}. *J. Superhard Mater.* **2023**, *45*, 239-248.

45. Mahat, S.; Li, S.; Wu, H.; Koirala, P.; Lv, B.; Cahill, D.G. Elastic constants of cubic boron phosphide and boron arsenide. *Phys. Rev. Mater*. **2021**, *5*, 033606.

46. Tian, F.; Luo, K.; Xie, C.; Liu, B.; Liang, X.; Wang, L.; Gamage, G.A.; Sun, H.; Ziyaee, H.; Sun, J.; Zhao, Z; Xu, B.; Gao, G.; Zhou, X.-F.; Ren, R. Mechanical properties of boron arsenide single crystal. *Appl. Phys. Lett*. **2019**, *114*, 131903.

47. Solozhenko, V.L.; Matar, S.F. Prediction of novel ultrahard phases in the B–C–N system from first principles: Progress and problems. *Materials* **2023**, *16*, 886

48. Brookes, C.A. The mechanical properties of cubic boron nitride. in *Proc. Int. Conf. Sci. Hard Mater.* **1986**, 207-220.

49. Solozhenko, V.L.; Bushlya, V. Mechanical properties of boron phosphides. *J. Superhard Mate*r. **2019**, *41*, 84-89.

50. Birch, F. Finite strain isotherm and velocities for single-crystal and polycrystalline NaCl at high pressures and 300 K. *J. Geophys. Res*. **1978**, *83*, 1257-1268.

51. Murnaghan F.D. The compressibility of media under extreme pressures. *Proc. Nation. Acad. Sci. USA* **1944**, *30*, 244-247.

52. Koshchenko, V.I.; Demidenko, A.F.; Grinberg, Ya.Kh.; Yachmenev, V.E. Specific-heats and thermodynamic functions of BP, BAs and B_6As at 5-310 K. *Izv. Akad. Nauk SSSR, Neorg. Mater.* **1981**, *17*, 1965-1968 (in Russian).

Table 1. Crystal structure parameters of BX (X = As, Sb, Bi) polymorphs.

	zb-BAs (Z = 4) *F*-43*m* (No. 216)	**qtz** BAs (Z = 3) $P6_422$ (No. 181)	*zb*-BSb (Z = 4) *F*-43*m* (No. 216)	**qtz** BSb (Z = 3) $P6_422$ (No. 181)	*zb*-BBi (Z = 4) *F*-43*m* (No. 216)	**qtz** BBi (Z = 3) $P6_422$ (No. 181)
a, Å	4.813 (4.777 [42])	3.461	5.279 (5.267 [43])	3.765	5.536 (5.528 [43])	3.944
c, Å	–	7.486	–	8.289	–	8.79252
V_{cell}, Å^3	111.51	77.66	146.97	101.78	169.65	118.46
V/FU, Å^3	27.88	25.89 ΔV/FU = 1.99	36.74	33.93 ΔV/FU = 2.81	42.41	39.49 ΔV/FU = 2.92
Shortest bond, Å	2.08	2.13	2.29	2.33	2.40	2.45
Angle (deg.)	109.47	108.42 / 90.74	109.47	108.41 / 90.74	109.47	106.76 / 91.93
Atomic positions	B (4c) ¼, ¼ , ¼ As (4a) 0, 0, 0	B (3c) ½, 0, 0 As (3d) ½, 0, ½	B (4c) ¼, ¼ , ¼ Sb (4a) 0, 0, 0	B (3c) ½, 0, 0 Sb (3d) ½, 0, ½	B (4c) ¼, ¼ , ¼ Bi (4a) 0, 0, 0	B (3c) ½, 0, 0 Bi (3d) ½, 0, ½
E_{total}, eV E_{total}/FU, eV	-45.47 -11.37	-31.44 -10.48 ΔE/FU= -0.89 eV	-40.14 -10.03	-28.01 -9.34 ΔE/FU= -0.69 eV	-35.69 -8.92	-25.06 -8.35 ΔE/FU= -0.57 eV

Table 2. Elastic constants C_{ij} of BX polymorphs. Bulk (B_V), shear (G_V) and Young's (E_V) moduli calculated by the Voight averaging. All values are in GPa.

	C_{11}	C_{12}	C_{13}	C_{33}	C_{44}	C_{66}	B_V	G_V	E_V
zb-BAs	268	67	67	268	146	146	134	128	291
qtz BAs	323	38	57	307	143	160	140	146	324
zb-BSb	182	58	58	182	97	97	99	83	195
qtz BSb	214	31	57	223	91	114	105	98	223
zb-BBi	124	39	39	124	67	67	67	57	134
qtz BBi	135	49	39	152	43	72	75	57	137

Table 3. Mechanical properties of BX polymorphs: Vickers hardness (H_V), bulk modulus (B), shear modulus (G_V), Young's modulus (E_V), Poisson's ratio (ν) and fracture toughness (K_{Ic})

	H_V				B		G_V	E_V	ν^{**}	$K_{Ic}^{\ddagger}$
	T*	LO†	MO‡	CN§	B_0*	B_V				
	GPa									MPa·m$^{1/2}$
zb-BAs [#216]	24	22	22	29	146	134	128	291	0.138	1.4
qtz BAs [#180]	25	22	27	36	154	140	146	324	0.113	1.2
zb-BSb [#216]	18	16	12	19	107	99	83	195	0.173	1.0
qtz BSb [#180]	19	9	16	24	116	105	98	223	0.149	1.0
zb-BBi [#216]	14	12	8	15	86	67	57	134	0.169	0.6
qtz BBi [#180]	15	7	7	12	92	75	57	137	0.197	0.6

* Thermodynamic model [36]

† Lyakhov-Oganov model [37]

‡ Mazhnik-Oganov model [34]

§ Chen-Niu model [35]

** ν values calculated using isotropic approximation

Table 4. Calculated properties of BX polymorphs: bulk moduli (B_0); total energies (E_0) and equilibrium volumes (V_0) per formula unit; *zb*-to-**qtz** transition pressures (p_{tr}) and corresponding reduced volumes (V_{tr}/V_0)

	BAs		BSb		BBi	
	zb	**qtz**	*zb*	**qtz**	*zb*	**qtz**
B_0 (GPa)	146*	154	107	116	86	92
E_0/FU (eV)	-11.37	-10.45	-10.06	-9.32	-8.92	-8.34
V_0/FU (Å^3)	27.88†	25.89	36.74	33.93	42.41	39.47
V_{tr}/V_0	0.697		0.724		0.763	
p_{tr} (GPa)	117		71		51	

* Experimental values: B_0 = 148(6) GPa and B_0' = 3.9(3) [15]; B_0 = 148(9) GPa [45]

† Experimental value: V_0/FU = 27.26 Å^3 [42]

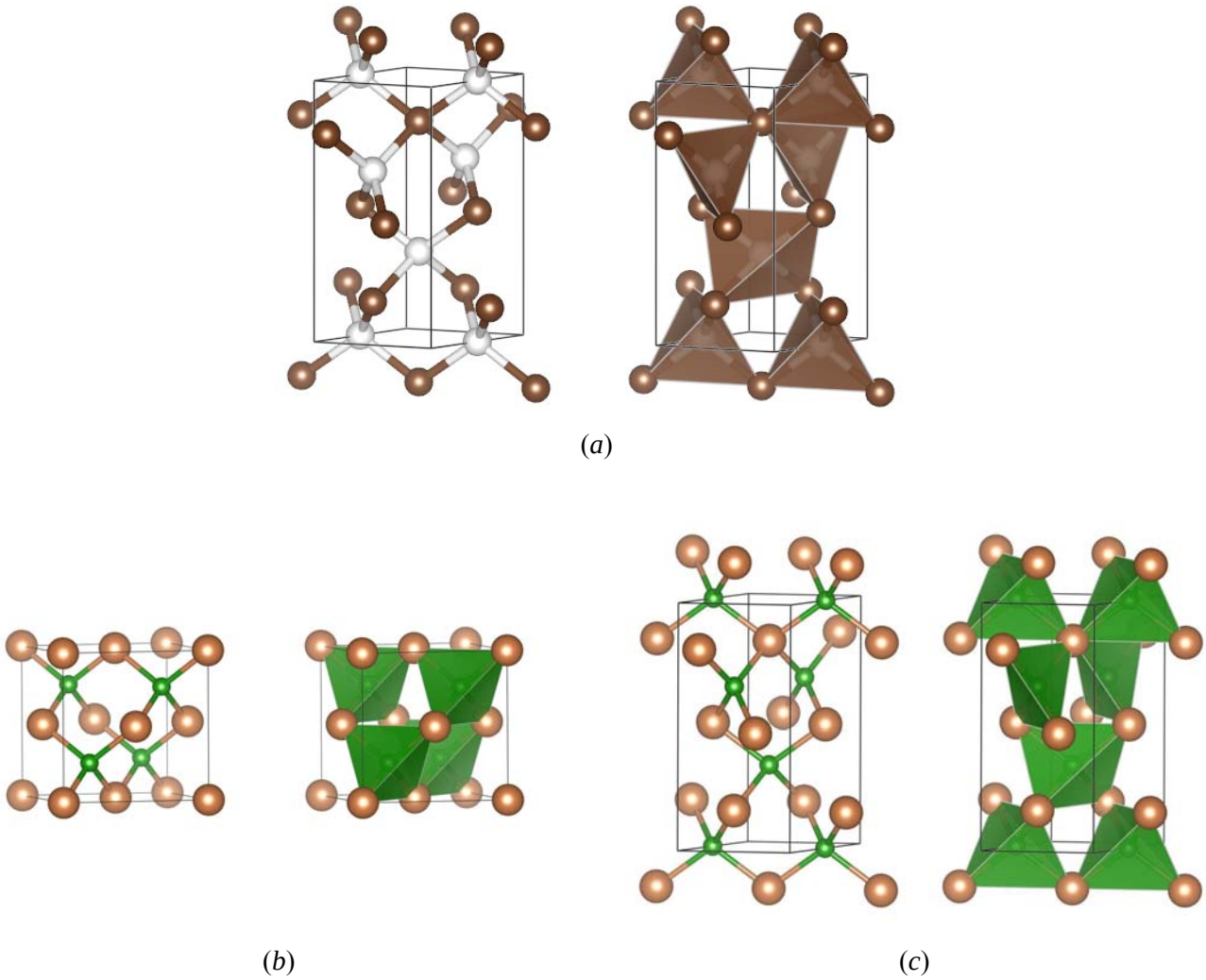

(*a*)

(*b*) (*c*)

Figure 1. Ball-and-stick and tetrahedral representations of the template **qtz** C_6 (space group $P6_222$) [44], in which two carbon substructures C1 (3c) (white spheres) and C2 (3d) (brown spheres) allow to accommodate two different types of atomic constituents to form hexagonal (**qtz**) structure of boron pnictides BX (X = As, Sb, Bi) (*c*), Cubic (zinc-blende) BX structure (*b*) is shown for comparison. Green and brick spheres correspond to B and X atoms, respectively.

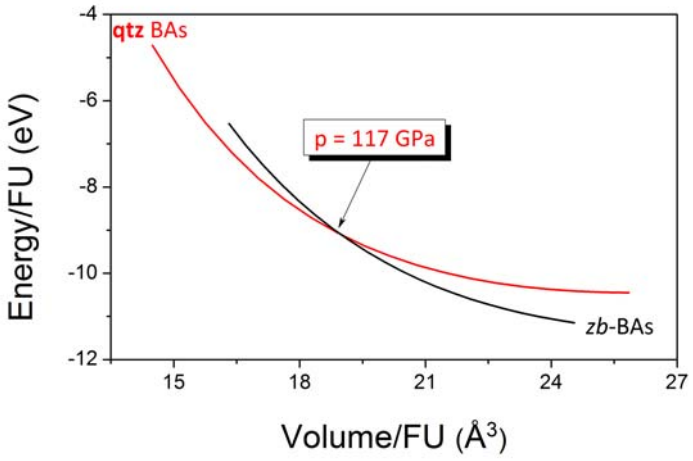

(*a*)

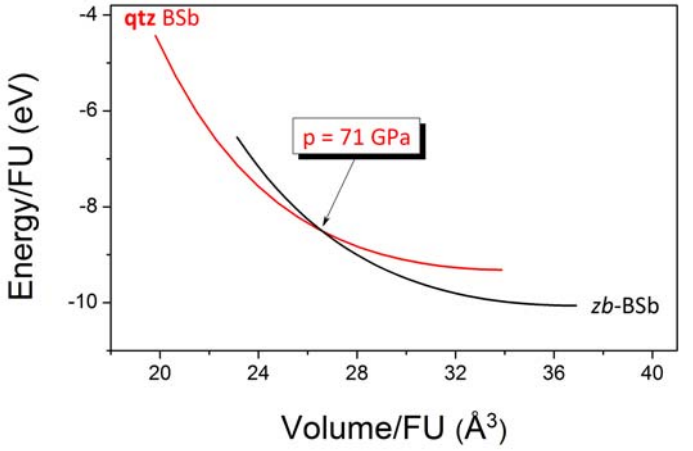

(*b*)

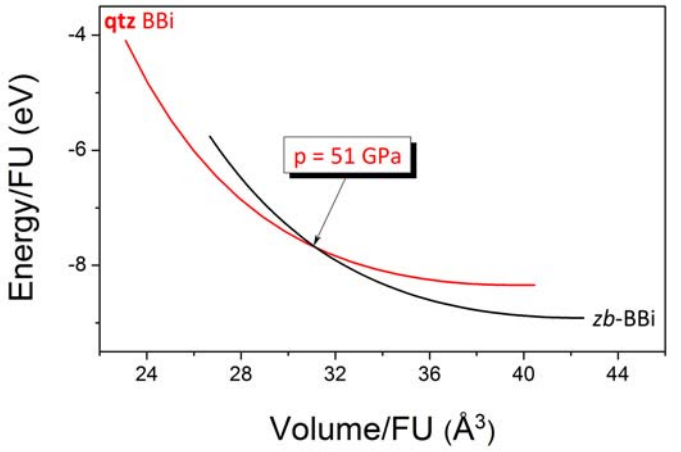

(*c*)

Figure 2. Calculated total energy per formula unit as a function of volume for zinc-blende and **qtz** boron pnictides: BAs (*a*), BSb (*b*), and BBi (*c*).

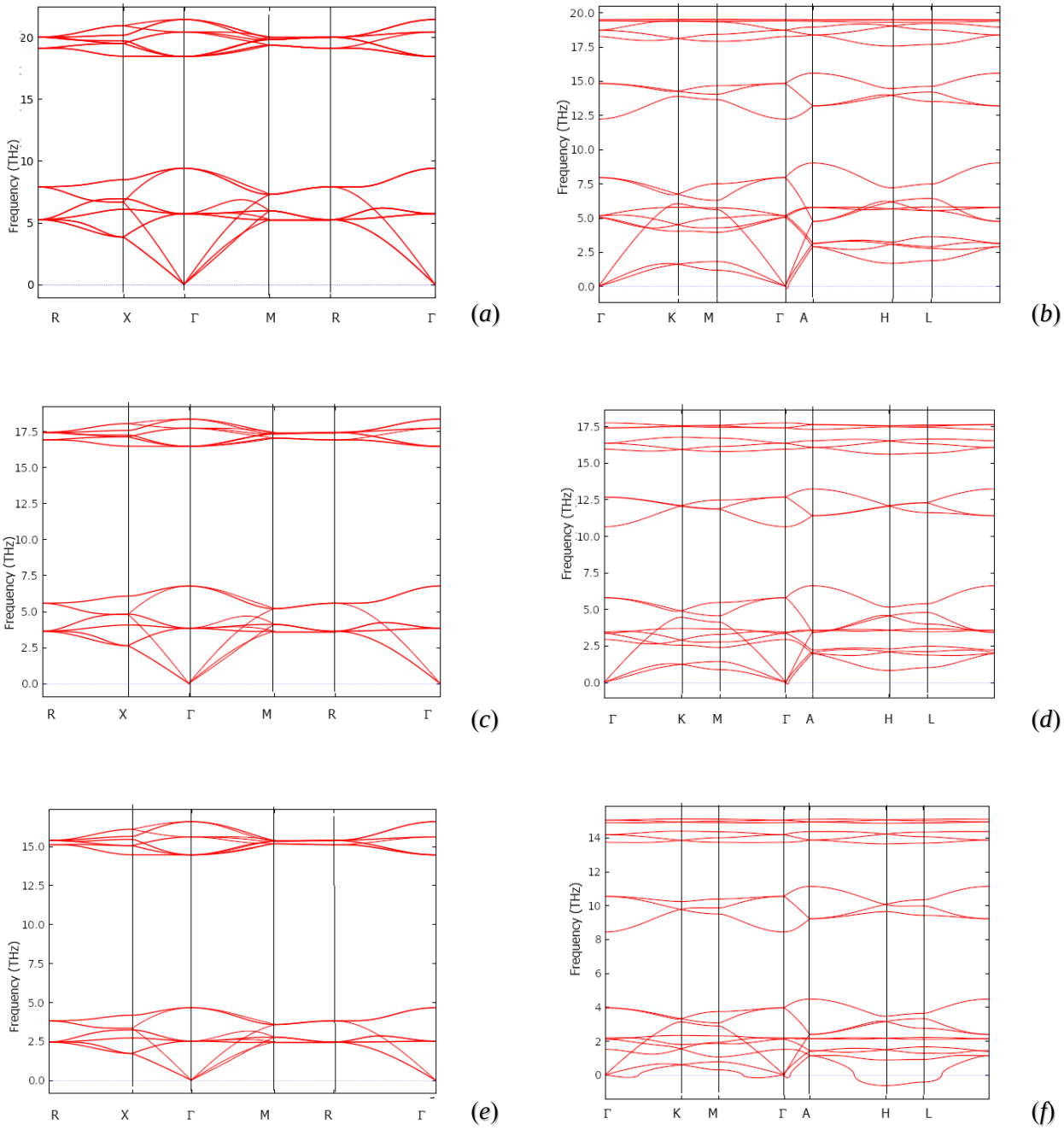

Figure 3. Phonon band structures of *zb*-BAs (*a*); **qtz** BAs (*b*); *zb*-BSb (*c*); **qtz** BSb (*d*); *zb*-BBi (*e*), and **qtz** BBi (*f*).

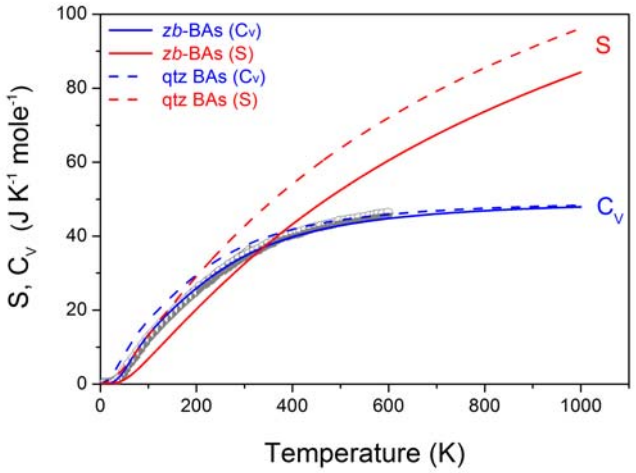

(*a*)

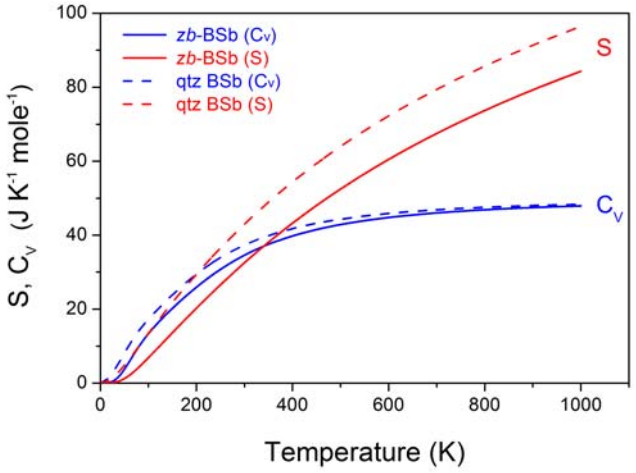

(*b*)

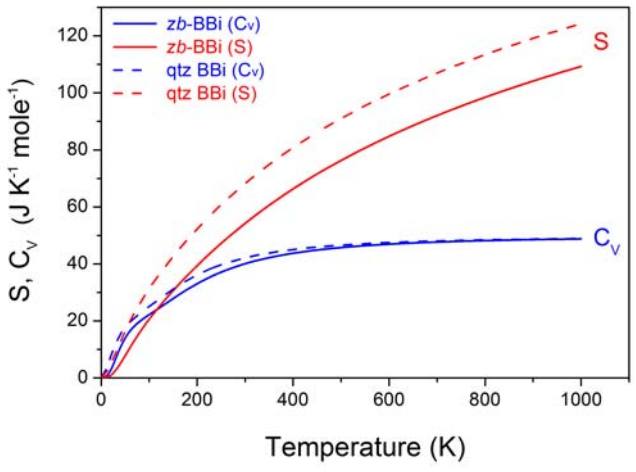

(*c*)

Figure 4. Heat capacity at constant volume (C_V) and entropy (S) of zinc-blende and **qtz** boron pnictides as functions of temperature: BAs (*a*), BSb (*b*) and BBi (*c*). Experimental heat capacity data for *zb*-BAs [2,52] are shown as gray symbols.

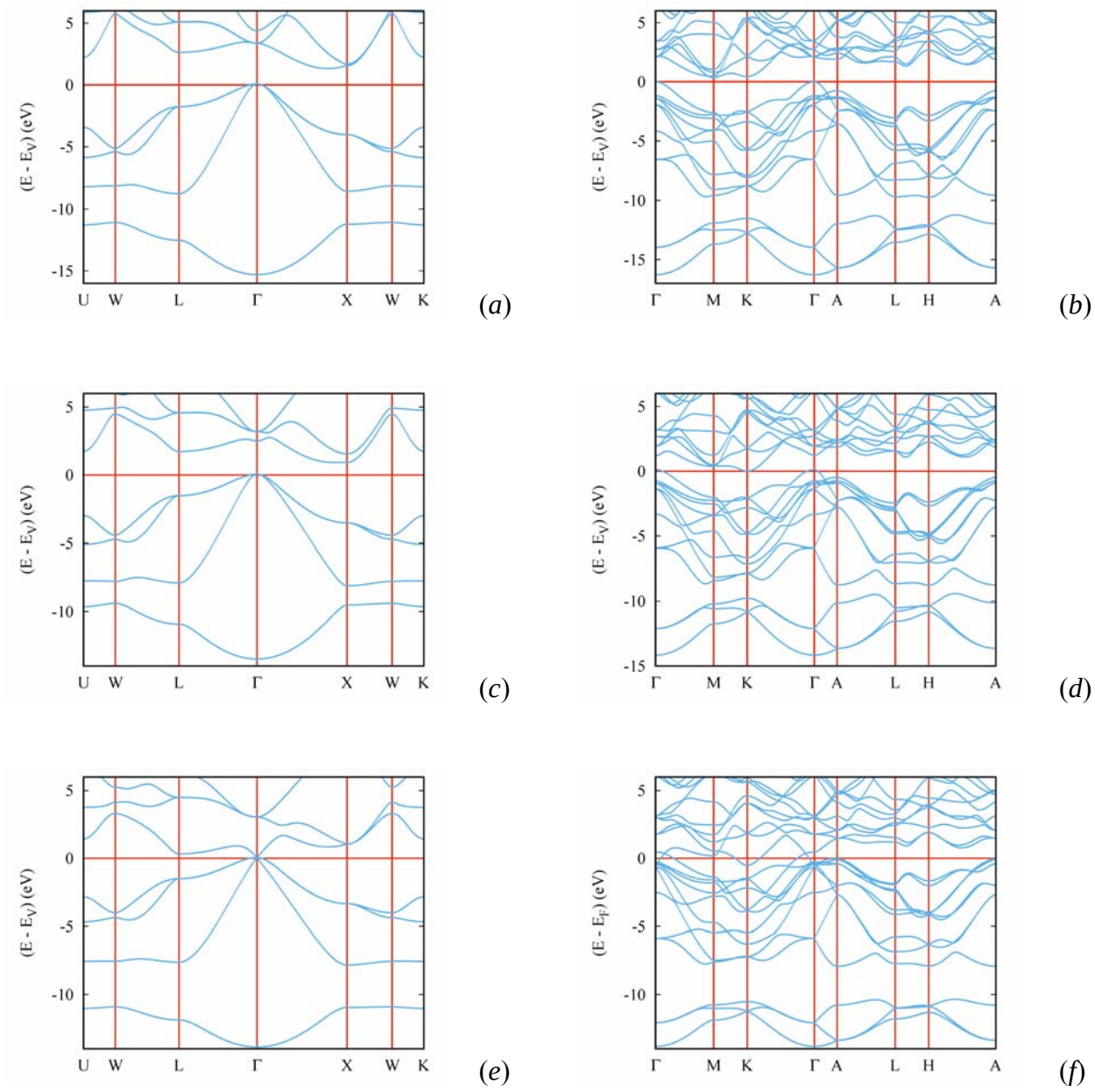

Figure 5. Electronic band structures of *zb*-BAs (*a*); **qtz** BAs (*b*); *zb*-BSb (*c*); **qtz** BSb (*d*); *zb*-BBi (*e*), and **qtz** BBi (*f*).